14th International Symposium on Turbulence and Shear Flow Phenomena (TSFP14)
Heidelberg, Germany, July 28–31, 2026

INFLUENCE OF CLUSTERING OF BARNACLE-LIKE ROUGHNESS ON DRAG AND TURBULENCE

Sina Nozarian
Mechanical and Production Engineering Department
Aarhus University
8200 Aarhus N, Denmark
nozarian@mpe.au.dk

Mahdi Abkar
Mechanical and Production Engineering Department
Aarhus University
8200 Aarhus N, Denmark
abkar@mpe.au.dk

Pourya Forooghi
Mechanical and Production Engineering Department
Aarhus University
8200 Aarhus N, Denmark
forooghi@mpe.au.dk

ABSTRACT

Direct numerical simulations (DNS) of turbulent channel flow at $\mathrm{Re}_\tau = 395$ are performed to quantify how spatial clustering of barnacle-like roughness modifies drag and near-wall turbulence at fixed global frontal solidity λ_f, defined as the ratio of the total projected frontal area of the elements (normal to the mean flow direction) to the planar wall area. Identical truncated-cone elements are arranged either uniformly at random or clustered using a gamma-distribution placement algorithm, at $\lambda_f = 0.045$ and 0.11. All rough cases exhibit a downward shift of the mean velocity profile relative to the smooth-wall reference, while retaining an approximately logarithmic behavior above the roughness crests. At matched λ_f, strong clustering reduces the roughness function and skin-friction drag compared with the random arrangement. Triple-decomposed statistics show that clustering amplifies dispersive stresses within the roughness layer, whereas increasing λ_f decreases the peak dispersive stress despite increasing drag. Time-averaged velocity fields at $y^+ = 30$ reveal pronounced high-speed corridors between clusters and intensified wake regions within clusters, providing a physical link between mean-flow heterogeneity and the observed arrangement sensitivity.

INTRODUCTION

Maritime transport is the backbone of international trade, carrying over 80% of globally traded goods by volume (UN Trade and Development (UNCTAD), 2024). For many hull forms a large fraction of the total resistance arises from skin-friction drag, making hydrodynamic efficiency highly sensitive to hull surface condition. Biofouling, including hard calcareous organisms such as barnacles, increases the effective roughness of the hull and can induce substantial powering penalties (Schultz, 2007; Schultz *et al.*, 2011). From a turbulence perspective, roughness alters near-wall dynamics and introduces additional length scales, making predictive drag modeling for realistic rough surfaces a persistent challenge (Jiménez, 2004; Flack & Schultz, 2014; Chung *et al.*, 2021).

The canonical description of rough-wall flows builds on the classical pipe measurements of Nikuradse (1933) and subsequent boundary-layer formulations introducing a roughness-induced downward shift of the inner-scaled mean velocity profile known as the Hama roughness function (Hama, 1954). Modern syntheses emphasize (i) the approximate outer-layer similarity of many rough-wall flows and (ii) the lack of a universal roughness length scale across textures and regimes (Jiménez, 2004; Flack & Schultz, 2010, 2014; Chung *et al.*, 2021). For discrete, three-dimensional roughness, density metrics such as frontal solidity are often informative because increasing density initially increases form drag, while at higher densities mutual sheltering can reduce incremental drag increases (Sarakinos & Busse, 2022; Womack *et al.*, 2022).

A key complication for marine biofouling is that roughness is rarely statistically homogeneous. Instead, organisms often appear in irregular colonies and clusters, implying spatially heterogeneous forcing of the near-wall flow. Spanwise or patchwise heterogeneity is known to generate roughness-induced inhomogeneities, persistent secondary motions, and modified momentum transport (Barros & Christensen, 2014; Anderson *et al.*, 2015; Wangsawijaya *et al.*, 2020). Recently, Jensen & Forooghi (2025) studied turbulent channel flow over prescribed patchy roughness and showed that heterogeneity length scale and coverage can significantly alter drag and turbulence statistics. The present work focuses on a related, but distinct, class of heterogeneity relevant to biofouling: irregular *clustering* of barnacle-like elements with gradual transitions between locally dense and sparse regions. By comparing clustered and uniformly random arrangements at matched global λ_f, we isolate the role of spatial organization in addition to roughness density.

DIRECT NUMERICAL SIMULATION SETUP

DNS of incompressible turbulent channel flow are performed using the pseudo-spectral solver SIMSON (Chevalier *et al.*, 2007). Fourier discretization is employed in the streamwise and spanwise directions and Chebyshev polynomials in the wall-normal direction. Nonlinear terms are advanced explicitly using a third-order Runge–Kutta method, while viscous terms are treated implicitly with a Crank–Nicolson scheme. The computational domain has dimensions $L_x \times L_y \times L_z = 2\pi\delta \times 2\delta \times \pi\delta$, where δ is the channel half-height, with periodic boundary conditions in x and z and no-slip conditions on both walls. The flow is driven by a constant mean pressure gradient and simulated at fixed friction Reynolds number $\mathrm{Re}_\tau = 395$. Roughness elements are mounted on both walls; the no-slip condition on the roughness geometry is enforced using an immersed boundary method following Goldstein *et al.* (1993). The numerical parameters are summarized in Table 1, and the surface cases are listed in Table 2.

The roughness elements are truncated cones intended to mimic sessile barnacles (Sadique, 2016). All elements have identical height k such that $k = 0.1\delta$ and $k^+ = ku_\tau/\nu = 39.5$, where u_τ is the friction velocity, and ν is the kinematic viscosity. The element planform parameters, the base radius and tip radius, are kept fixed at 0.135δ and 0.045δ, respectively, across all cases, following geometries similar to those in (Sarakinos & Busse, 2022; Nozarian *et al.*, 2024); only the element *locations* differ. Two global frontal solidities are studied, $\lambda_f = 0.045$ and 0.11, where λ_f denotes the ratio of the total projected frontal area of the elements (normal to the mean flow direction) to the planar wall area.

Uniformly random cases (RN) are generated by sampling element centers from a uniform distribution in (x, z) with a non-overlap constraint. Clustered cases (CL) are constructed by distributing elements around two prescribed cluster centers located at $(x_c, z_c) = (\pi/2, \pi/4)$ and $(3\pi/2, 3\pi/4)$ in units of δ, where the radial distance r from a cluster center is sampled from a gamma distribution with probability density function

$$f(r; K, \theta) = \frac{r^{K-1}\exp(-r/\theta)}{\theta^K \Gamma(K)}, \qquad r > 0, \tag{1}$$

in which K is the shape parameter, θ is the scale parameter, and $\Gamma(K)$ is the Gamma function. In this study, K is fixed at 2.0, while θ is varied (0.15 and 0.30) to control clustering intensity, with smaller θ producing tighter clusters.

The overall skin-friction coefficient is defined as

$$C_f = \frac{2\tau_w}{\rho U_b^2}, \tag{2}$$

where $\tau_w = \rho u_\tau^2$ is the mean effective wall shear stress, and U_b is the bulk velocity. The Hama roughness function ΔU^+ is computed as the downward shift of the rough-wall mean velocity profile relative to the smooth-wall reference at the same

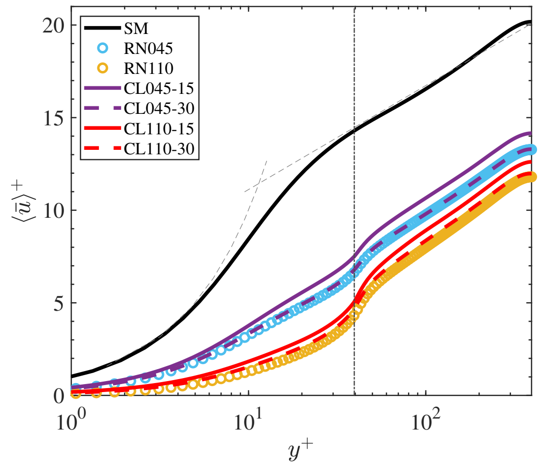

Figure 1. Mean streamwise velocity profiles for the smooth-wall reference (SM) and rough-wall cases. The vertical dash-dotted line indicates the roughness height $k^+ = 39.5$.

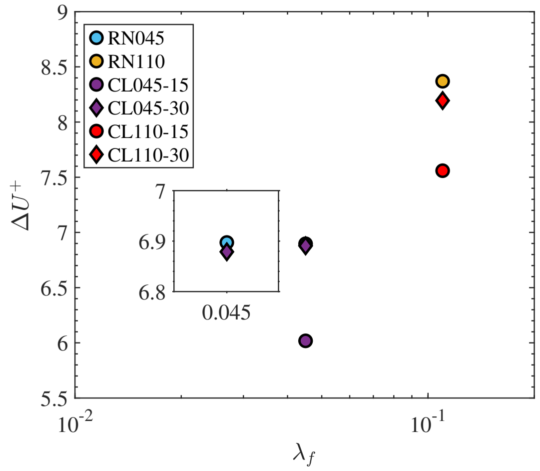

Figure 2. Hama roughness function ΔU^+ versus frontal solidity λ_f for random (RN) and clustered (CL) surfaces at $\mathrm{Re}_\tau = 395$.

Re_τ, obtained here from the difference in centerline velocities,

$$\Delta U^+ = U^+_{c,\mathrm{smooth}} - U^+_{c,\mathrm{rough}}. \tag{3}$$

where $(\cdot)^+$ denotes viscous scaling with u_τ and ν. In this paper $\overline{(\cdot)}$ denotes temporal averaging and $\langle(\cdot)\rangle$ denotes wall-parallel (x–z) averaging; hence $\langle\overline{u}\rangle(y)$ is the time- and plane-averaged mean velocity.

RESULTS AND DISCUSSION

Mean velocity profiles and roughness function

Figure 1 presents the inner-scaled mean streamwise velocity profile, $\langle\overline{u}\rangle^+$, for the smooth-wall reference and all rough-wall cases. As expected, all rough surfaces exhibit a characteristic downward shift relative to the smooth-wall profile, indicating increased skin-friction drag. At the same time, the mean profiles retain an approximately logarithmic behavior above the roughness crests, located at $k^+ = 39.5$, consistent

Table 1. DNS parameters at $\mathrm{Re}_\tau = 395$. Spatial parameters are normalized by the channel half-height δ.

Configuration	L_x/δ	L_z/δ	$N_x \times N_y \times N_z$	Δx^+	Δz^+	$\Delta y^+_{\mathrm{min}}$	$\Delta y^+_{\mathrm{max}}$
Smooth	2π	π	$256 \times 193 \times 192$	9.7	4.8	0.05	6.4
Rough	2π	π	$768 \times 301 \times 384$	3.2	3.2	0.02	4.1

Table 2. Surface cases at $\mathrm{Re}_\tau = 395$. All rough cases have identical truncated-cone geometry with $k/\delta = 0.1$ ($k^+ = 39.5$). Case names follow RNλ_f for random placement and CLλ_f-100θ for clustered placement with gamma-distribution parameters $K = 2.0$ and scale θ.

Case	Arrangement	λ_f	θ	K	ΔU^+	C_f
SM	Smooth	—	—	—	—	0.006
RN045	Random	0.045	—	—	6.89	0.017
RN110	Random	0.110	—	—	8.36	0.024
CL045-15	Clustered	0.045	0.15	2.0	6.01	0.014
CL045-30	Clustered	0.045	0.30	2.0	6.78	0.017
CL110-15	Clustered	0.110	0.15	2.0	7.55	0.020
CL110-30	Clustered	0.110	0.30	2.0	8.19	0.022

with canonical rough-wall turbulence (Jiménez, 2004; Flack & Schultz, 2014; Chung *et al.*, 2021). Comparing cases with the same frontal solidity, no appreciable differences are observed extremely close to the wall; the profiles for RN and CL cases at matched λ_f remain nearly indistinguishable up to approximately $y^+ \approx 10$. Beyond this wall-normal distance, the effect of roughness *arrangement* becomes apparent, and the mean profiles begin to separate, indicating that spatial organization primarily modulates the flow within and just above the roughness layer, defined here as the region between the smooth settling plane and the roughness crests, following the definition of Sarakinos & Busse (2022).

Variations in frontal solidity λ_f produce clear differences in the mean profiles, including in the near-wall region, with the higher-solidity cases displaying a larger velocity deficit relative to the smooth-wall reference. This observation is consistent with prior studies reporting increasing roughness influence with increasing element density (e.g. Sarakinos & Busse, 2022).

The corresponding Hama roughness function ΔU^+ is summarized in figure 2 and reported together with C_f in Table 2. In general, ΔU^+ increases with increasing λ_f for the present range of solidities, in agreement with the widely reported trend that increasing frontal solidity strengthens the roughness-induced velocity deficit (Jiménez, 2004). Previous work has also suggested that beyond a case-dependent critical solidity, increased packing can lead to a reduction in the incremental drag increase due to sheltering effects (e.g. MacDonald *et al.*, 2016; Placidi & Ganapathisubramani, 2015; Sarakinos & Busse, 2022). In the present study, the maximum solidity is $\lambda_f = 0.11$, which lies below the proposed critical values, and a consistent increase of ΔU^+ is therefore observed when comparing the $\lambda_f = 0.045$ and 0.11 groups.

At fixed λ_f, clustering modifies the drag response in a systematic manner. For $\lambda_f = 0.045$, the weakly clustered case (CL045-30) yields a roughness function close to the uniformly random surface (RN045), whereas the strongly clustered case (CL045-15) exhibits a noticeably lower ΔU^+ and correspondingly reduced skin-friction, as reflected by the values in Table 2. At $\lambda_f = 0.11$, the separation among arrangements becomes more pronounced: RN110 shows the largest ΔU^+, the weakly clustered CL110-30 remains close but slightly lower, and the strongly clustered CL110-15 displays a substantial reduction in ΔU^+ and C_f. Overall, these results demonstrate that while λ_f largely controls the magnitude of the mean velocity shift, spatial organization, and in particular strong clustering, yields reduced skin-friction drag at fixed global solidity relative to the uniformly random cases, highlighting the need for descriptors beyond global density to characterize heterogeneous barnacle-like roughness.

Canopy mean-flow imprint

Figure 3 visualizes the time-averaged streamwise velocity field at $y^+ = 30$, i.e. below the roughness crest. For uniformly random arrangements, the modulation of the mean field is comparatively homogeneous at each λ_f, with distributed low-speed regions associated with element wakes and no persistent large-scale preferential pathways. Clustering introduces pronounced organization of the canopy flow: dense clusters generate extended low-speed wake regions, while the intervening sparse regions form high-speed "channels" that provide preferential pathways for momentum. These coherent high- and low-speed regions become more distinct with increasing clustering intensity, providing a qualitative explanation for the arrangement sensitivity observed in the mean velocity shift (Fig. 1) and roughness function (Fig. 2). Moreover, the strong spatial modulation evident for the clustered cases anticipates an enhanced dispersive contribution in the roughness layer, which is quantified below using a triple decomposition.

Triple decomposition

To separate the contributions of temporal and spatial fluctuations arising from roughness-induced inhomogeneities, a triple decomposition (Raupach & Shaw, 1982) is applied to the velocity field. For the streamwise velocity component $u(x,y,z,t)$,

$$u(x,y,z,t) = \langle \overline{u} \rangle(y) + \tilde{u}(x,y,z) + u''(x,y,z,t), \tag{4}$$

where $\langle \overline{u} \rangle(y)$ is the time and plane-averaged velocity, $\tilde{u}(x,y,z) = \overline{u}(x,y,z) - \langle \overline{u} \rangle(y)$ is the dispersive (spatial) deviation of the time-averaged flow, and $u''(x,y,z,t) = u - \overline{u}$ is the turbulent fluctuation about the local time mean. This decomposition isolates roughness-induced coherent inhomogeneity

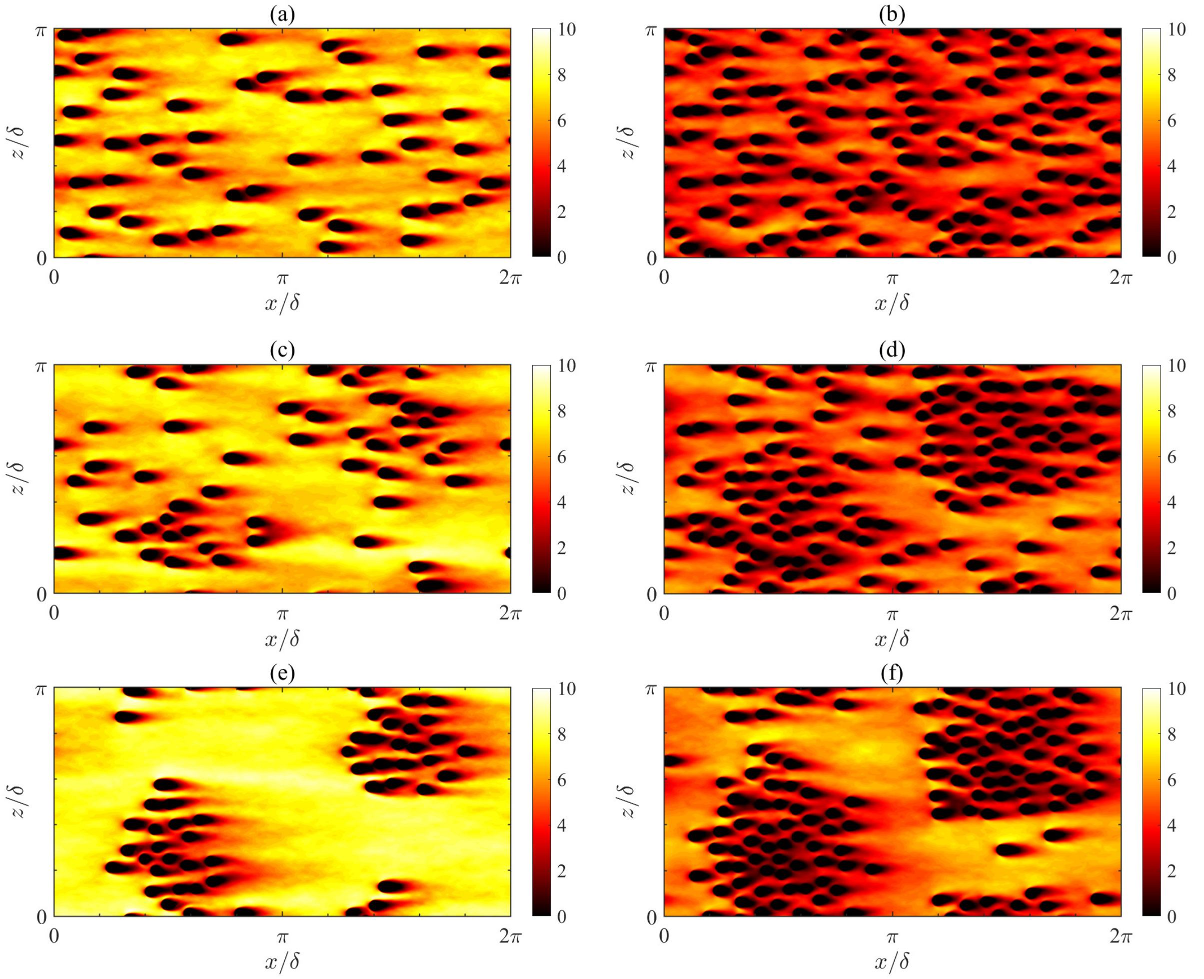

Figure 3. Time-averaged streamwise velocity at $y^+ = 30$ for all rough cases: (a,c,e) $\lambda_f = 0.045$ and (b,d,f) $\lambda_f = 0.11$. Rows correspond to random (a,b), weakly clustered (c,d), and strongly clustered (e,f). Element footprints and roughness-induced low-speed regions are apparent, while clustering produces extended high-speed pathways between clusters and intensified wakes within clusters.

(via dispersive stresses such as $\langle\tilde{u}\tilde{u}\rangle$) from turbulent motions (via Reynolds stresses such as $\langle u''u''\rangle$).

Reynolds and dispersive stresses

Figure 4 reports the streamwise Reynolds stress $\langle u''u''\rangle^+$ and the corresponding dispersive stress $\langle\tilde{u}\tilde{u}\rangle^+$ obtained from the triple decomposition. The vertical dash-dotted line marks the roughness height at $k^+ = 39.5$. In the outer layer the rough-wall cases collapse closely, indicating weak sensitivity to surface arrangement away from the wall and consistency with outer-layer similarity when scaled with u_τ and δ (Flack & Schultz, 2014; Chung *et al.*, 2021). The discussion below therefore focuses on the roughness layer and near-crest region.

In figure 4(a), all rough-wall cases exhibit a reduced near-wall streamwise turbulence intensity relative to the smooth-wall reference, consistent with disruption of the smooth-wall buffer-layer dynamics and redistribution of turbulence production within and above the roughness layer (Jiménez, 2004; Sarakinos & Busse, 2022). The rough-wall profiles display a pronounced maximum located just above the roughness crests, at $y^+ \approx 45$, and this peak location is essentially insensitive to arrangement and λ_f for the present cases. However, the magnitude of the peak depends on both solidity and organization: increasing λ_f from 0.045 to 0.11 generally reduces the peak level, and at fixed λ_f the clustered cases attain higher $\langle u''u''\rangle^+$ than the corresponding random case, with the strongest clustering producing the largest peak. A further feature at the lower solidity, $\lambda_f = 0.045$, is a weak but noticeable double-peak behavior: in addition to the outer maximum near $y^+ \approx 45$, a secondary local maximum appears around $y^+ \approx 14$, i.e. close to the location of the smooth-wall buffer-layer peak. This secondary peak is most pronounced for the strongly clustered case (CL045-15) and is weaker for the random and weakly clustered cases. The emergence of a near-smooth-wall peak location suggests that, at low global solidity, strong clustering creates extended inter-cluster corridors where the near-wall cycle partially recovers, superimposed on the roughness-induced peak associated with the canopy-shear layer. This interpretation is consistent with the time-averaged canopy-flow organization in figure 3, which shows more distinct high-speed pathways between clusters for the strongly clustered surface.

The dispersive stresses in figure 4(b) are strongly confined to the roughness layer and provide a direct measure of roughness-induced spatial inhomogeneity in the time-averaged flow (Raupach & Shaw, 1982). As expected, $\langle\tilde{u}\tilde{u}\rangle^+$ peaks below or near the crest height, reflecting the strongest spatial modulation of the mean streamwise velocity within the canopy

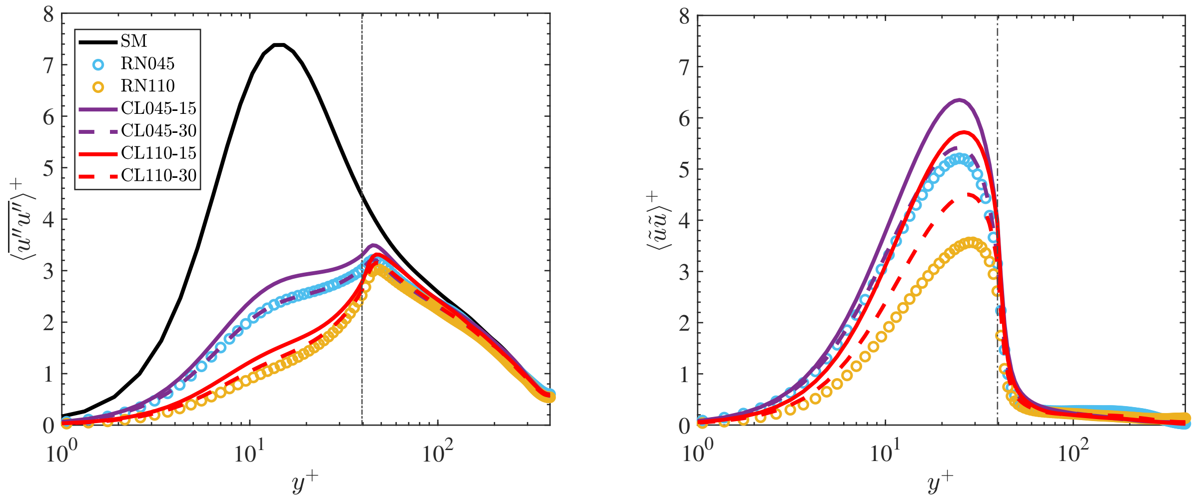

Figure 4. Streamwise (a) Reynolds stresses $\langle u''u'' \rangle^+$ and (b) dispersive stresses $\langle \tilde{u}\tilde{u} \rangle^+$ from triple decomposition. The vertical dash-dotted line indicates the roughness height $k^+ = 39.5$.

and immediately above it. At fixed λ_f, the peak magnitude increases systematically with clustering intensity: the random arrangements yield the lowest values, while the clustered cases exhibit substantially larger peaks, with the strongly clustered cases attaining the largest dispersive stresses. This hierarchy is consistent with the canopy-flow visualizations in figure 3, where clustered surfaces generate pronounced low-speed regions within clusters and high-speed corridors between clusters, thereby strengthening spatial variations in $\bar{u}$ and elevating $\langle \tilde{u}\tilde{u} \rangle^+$.

When comparing across the two solidities, the overall peak level of $\langle \tilde{u}\tilde{u} \rangle^+$ is higher for $\lambda_f = 0.045$ than for $\lambda_f = 0.11$ for each arrangement class. This decrease with an increasing λ_f suggests that, for the present geometries, the denser surfaces produce a more uniformly obstructed near-wall region that limits persistent bypass pathways and reduces the amplitude of spatial modulation in the time-averaged flow, even though the mean drag increases (cf. Table 2). In other words, increasing λ_f increases the skin-friction drag, but it reduces the peak streamwise dispersive stress. This shows that drag and dispersive stress do not necessarily change monotonically together, and that the roughness arrangement is the primary control on mean-flow heterogeneity within the roughness layer.

CONCLUSIONS

DNS of turbulent channel flow at $\mathrm{Re}_\tau = 395$ were used to isolate how clustering of barnacle-like roughness elements affects drag and near-wall turbulence at fixed global frontal solidity. Across all rough cases, the mean streamwise velocity exhibits a clear downward shift relative to the smooth-wall reference while maintaining an approximately logarithmic behavior above the roughness crests. At fixed λ_f, spatial organization is found to be a key control parameter: strong clustering reduces the roughness function ΔU^+ and the skin-friction coefficient relative to the random arrangement (Table 2). For the low-solidity cases, the streamwise Reynolds stress exhibits a weak double-peak behavior, including a secondary maximum near the smooth-wall buffer-layer location ($y^+ \approx 14$), most pronounced for the strongly clustered surface, suggesting partial recovery of near-wall dynamics in inter-cluster corridors.

Statistics show that dispersive stresses are confined to the roughness layer and increase systematically with clustering intensity at each λ_f, consistent with enhanced spatial modulation of the time-averaged flow. In contrast, the peak dispersive stress decreases when λ_f increases from 0.045 to 0.11, indicating that denser surfaces can become more uniformly obstructing and thereby reduce the amplitude of mean-flow heterogeneity even as drag increases. Time-averaged velocity fields at $y^+ = 30$ support this interpretation by revealing pronounced high-speed pathways between clusters and intensified low-speed wake regions within clusters.

Overall, the results demonstrate that global density measures such as λ_f do not uniquely determine either drag or the structure of the roughness layer for heterogeneous barnacle-like roughness. Incorporating descriptors of spatial organization (e.g. clustering intensity) is therefore essential for predictive modeling of biofouling-induced drag.

REFERENCES

Anderson, William, Barros, Julio M., Christensen, Kenneth T. & Awasthi, Ankit 2015 Numerical and experimental study of mechanisms responsible for turbulent secondary flows in boundary layer flows over spanwise heterogeneous roughness. *J. Fluid Mech.* **768**, 316–347.

Barros, Julio M. & Christensen, Kenneth T. 2014 Observations of turbulent secondary flows in a rough-wall boundary layer. *J. Fluid Mech.* **748**, R1.

Chevalier, M., Schlatter, P., Lundbladh, A. & Henningson, D. S. 2007 A pseudo-spectral solver for incompressible boundary layer flows. Exec. summary and final report. KTH Mech., Stockholm, Sweden, tech. Rep. TRITA-MEK 2007:7.

Chung, Daniel, Hutchins, Nicholas, Schultz, Michael P. & Flack, Karen A. 2021 Predicting the drag of rough surfaces. *Annu. Rev. Fluid Mech.* **53**, 439–471.

Flack, Karen A. & Schultz, Michael P. 2010 Review of hydraulic roughness scales in the fully rough regime. *J. Fluids Eng.* **132** (4), 041203.

Flack, Karen A. & Schultz, Michael P. 2014 Roughness effects on wall-bounded turbulent flows. *Phys. Fluids* **26** (10), 101305.

Goldstein, D., Handler, R. & Sirovich, L. 1993 Modeling a no-slip flow boundary with an external force field. *J. Comput. Phys.* **105** (2), 354–366.

Hama, F. R. 1954 Boundary-layer characteristics for smooth and rough surfaces. *Tech. Rep.*. Hughes Aircraft Co., report; introduced the roughness function concept for boundary layers.

Jensen, N. & Forooghi, P. 2025 A study of turbulent flow over patchy roughness. *J. Fluid Mech.* **1006**, A28.

Jiménez, Javier 2004 Turbulent flows over rough walls. *Annu. Rev. Fluid Mech.* **36**, 173–196.

MacDonald, M., Chan, L., Chung, D., Hutchins, N. & Ooi, A. 2016 Turbulent flow over transitionally rough surfaces with varying roughness densities. *J. Fluid Mech.* **804**, 130.

Nikuradse, J. 1933 Laws of flow in rough pipes. *VDI-Forsch.-h.* **361**, english translation commonly cited in roughness literature.

Nozarian, S., Abkar, M. & Forooghi, P. 2024 An analysis of drag reduction using spanwise forcing on rough walls. *Int. J. Heat Fluid Flow.* **106**, 109306.

Placidi, M. & Ganapathisubramani, B. 2015 Effects of frontal and plan solidities on aerodynamic parameters and the roughness sublayer in turbulent boundary layers. *J. Fluid Mech.* **782**, 541.

Raupach, M. R. & Shaw, R. H. 1982 Averaging procedures for flow within vegetation canopies. *Bound.-Layer Meteorol.* **22**, 79–90.

Sadique, J. 2016 Turbulent flows over macro-scale roughness elements—from biofouling barnacles to urban canopies. PhD thesis, Johns Hopkins Univ., Baltimore, MD.

Sarakinos, Georgios & Busse, Angela 2022 Turbulent channel flow over barnacle-like roughness: the effect of roughness solidity and arrangement. *Phys. Rev. Fluids* **7**, 064602.

Schultz, Michael P. 2007 Effects of coating roughness and biofouling on ship resistance and powering. *Biofouling* **23** (5–6), 331–341.

Schultz, M. P., Bendick, J. A., Holm, E. R. & Hertel, W. M. 2011 Economic impact of biofouling on a naval surface ship. *Biofouling* **27** (1), 87–98.

UN Trade and Development (UNCTAD) 2024 Review of maritime transport 2024: Navigating maritime chokepoints. Accessed 2026-03-04.

Wangsawijaya, Dea D., Baidya, Rio, Chung, Daniel, Marusic, Ivan & Hutchins, Nicholas 2020 The effect of spanwise wavelength of surface heterogeneity on turbulent secondary flows. *J. Fluid Mech.* **894**, A7.

Womack, K. M., Volino, R. J., Meneveau, C. & Schultz, M. P. 2022 Turbulent boundary layer flow over regularly and irregularly arranged truncated cone surfaces. *J. Fluid Mech.* **933**, A38.